A novel control solution for improved trajectory tracking and LVRT performance in DFIG-based wind turbines

Control Theory and Technology

A Novel Control Solution for Improved Trajectory Tracking and LVRT Performance in DFIG-based Wind Turbines

Ahmad HASHEMI [1,2†], Christian CONFICONI [1], Andrea TILLI [1],

1. *The Center of Complex Automated Systems (CASY) at the Department of Electrical, Electronic and Information Engineering (DEI), University of Bologna, Risorgimento, 2, 40136 Bologna, Italy;*

2. *Sama Technical and Vocational training College, Islamic Azad University, Kermanshah Branch, Kermanshah, Iran*

Abstract:

This paper presents a new control strategy for the rotor side converter of Doubly-Fed Induction Generator based Wind Turbine systems, under severe voltage dips. The main goal is fulfilling the Low Voltage Ride Through performance, required by modern Grid Codes. In this respect, the key point is to limit oscillations (particularly on rotor currents) triggered by line faults, so that the system keeps operating with graceful performance. To this aim, a suitable feedforward-feedback control solution is proposed for the DFIG rotor side. The feedforward part exploits oscillation-free reference trajectories, analytically derived, for the system internal dynamics. State feedback, designed accounting for control voltage limits, endows the system with robustness and further tame oscillations during faults. Moreover, improved torque and stator reactive power tracking during faults is achieved, proposing an exact mapping between such quantities and rotor-side currents, which are conventionally used as controlled outputs. Numerical simulations are provided to validate the capability of the proposed approach to effectively cope with harsh faults.

Keywords: Doubly-fed induction generator (DFIG); Wind turbine (WT); Feedforward-feedback control; Mapping solution; Low voltage ride through (LVRT)

1 Introduction

Global installed renewable generation capacity has been consistently increasing in the last years, reaching a total of 1,985 GW at the end of 2015 [1]. Among renewables, wind power has been the fastest growing energy source, exponentially going from 6.1 GW in 1996 to 282.6 GW in 2012, and it is predicted to reach 760 GW by 2020 with the current trend [2].

Doubly-Fed Induction Generator (DFIG) is one of the most popular technologies for wind energy applications. Indeed, more than 50% of the currently installed Wind Energy Conversion Systems (WECSs) use this class of electrical machines [3]. Typical DFIG-based Wind Turbine (WT) configuration is shown in Fig.1. Stator is connected directly to grid, while rotor is fed by back-to-back Grid/Rotor Side Converters (GSC/RSC) allowing bidirectional power flow between the grid and generator rotor side. This topology allows WT variable speed control, with RSC managing a fraction (around 30%, but depending on slip value) of the overall generation system power. Thus, RSC has about one third of the size, cost and losses of a conventional variable-speed drive.

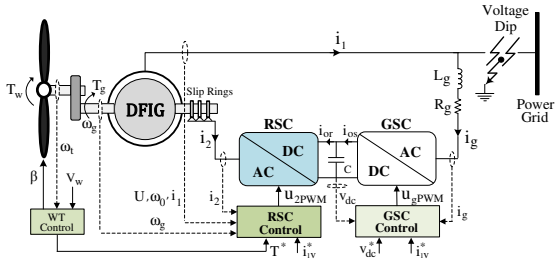

Fig. 1: General configuration of the studied DFIG WT system.

Given the mentioned high penetration, making WECSs critical sources of nowadays power networks, specific na-

†Corresponding author.

E-mail: [ahmad.hashemi, christian.conficoni3, andrea.tilli]@unibo.it. Tel.: +390512093924; fax: +390512093073.

tional Grid Codes have been issued, demanding such systems to comply with safety, reliability, and stable operation requirements. Achieving Low Voltage Ride Through (LVRT) capability for a predefined set of possible grid faults, is one of the most critical requirements. According to these specifications, during the voltage shortage, WECSs have to remain connected for a specific duration, supplying reactive power to the grid, to help sustaining the power network. Time period of LVRT depends on the dip magnitude at the Point of Common Coupling (PCC) and the time taken by the system to recover the pre-fault condition. As instances, German E.ON Netz regulations asks for riding through 85% voltage drop lasting for $625ms$, while American FERC accounts for 100% drop for $150ms$ [4], [5]. Line voltage dips reduce the power which can be injected into the grid, impairing the system energy balance. Consequently, to avoid the DC-link overvoltage due to GSC current limits, generator torque should be accordingly declined. In addition, since DFIG is extremely sensitive to grid voltage variations (because the stator is directly connected to the grid) voltage dips can trigger large electromagnetic transients leading to large stator/rotor flux/current oscillations. As a consequence, rotor-side controller gives large voltages on RSC, hitting converter limits, and eventually causing overcurrents on the rotor. Thus, RSC is disconnected to prevent damages, disrupting LVRT. Crowbar protection is the most conventional remedy to prevent rotor overcurrent in currently installed WTs [6–8]. However, crowbar system adds extra cost, furthermore it impairs DFIG's controllability (rotor is short-circuited through the protection resistances) hindering LVRT capabilities. In addition, triggering crowbar intervention makes the generator to absorb large reactive power from the grid. This worsens line voltage degradation, instead of supporting the network by reactive component injection as asked in Grid Codes [9].

To overcome these drawbacks, and endow WECSs with LVRT property, several strategies have been proposed. In [7], to bound oscillations within the grid voltage dip, the focus is put into storing imbalanced power into the WT kinetic energy, letting its speed to increase. In [10], DFIG reactive power support feature under grid faults is mainly considered. In [11], a protection hardware for in-grid DFIG, based on a resistive type superconducting fault current limiter (SFCL) connected in series with the DFIG rotor winding, is designed. In [12], during the grid fault, an Energy Storage Device (ESD) is utilized for DC-link voltage regulation, while GSC connection is reconfigured to be paralleled with RSC, providing an alternative path for the rotor current. In [13], during line faults, rotor current is controlled to track stator current in a certain scale, in order to achieve LVRT capacity and comply with the constraint of converter's maximum output voltage.

The main contribution of this work to such literature is to present a strategy to deal with line voltage faults only by means of advanced control techniques, limiting electromagnetic signals oscillations. In addition, a suitably accurate tracking of torque and reactive current references throughout the dip is ensured. This way, improved LVRT performance can be achieved, also for severe faults, with no additional protection hardware.

The solution is mainly focused on rotor-side control, which is the knob to be used to obtain the aforementioned properties. In this context, the framework of field-oriented control (see [14], [15] for applications to DFIG control in nominal scenarios) will serve as the base to design advanced strategies to deal with line faults. For what regards grid side control, the goal is simply to regulate the DC-link voltage, and well-established techniques exist [16], therefore it will not be detailed. However, it will be implemented and considered, along with power electronic converters non-idealities, WT and gearbox mechanics, and Maximum Power Point Tracking (MPPT) algorithm, for validation on a complete WECS benchmark via detailed simulations. In this context, a feedforward-feedback RSC control unit, first presented in [17], is exploited, assuming rotor currents as the controlled output variables. The feedforward terms are based on suitable oscillation-free state references which, in turn, are derived from a thoughtful analysis of the system internal dynamics behavior under line voltage sags. Removing DFIG natural oscillations from reference signals and feedforward part is crucial to successfully handle harsh dips. Then, in order to endow the controller with some robustness, to improve convergence towards the desired state trajectories, and to further limit oscillations under faults, a feedback part is designed according to modern saturated control techniques, in order to account for control inputs (rotor voltages) limits. Relying on such unit, an additional, novel key point presented here is an exact, analytical method to convert torque and stator reactive current references (the typical variables of interest for DFIG-based WT) into the corresponding rotor currents references. This improves tracking under line faults, with clear benefits on the system overall behavior under line dips.

The paper is organized as follows. In Section 2, DFIG and WT models are reported, and a general outline of MPPT algorithm is presented. In Section 3, control objectives and system physical limits are explained. Then, the pro-

posed RSC control is deduced. Starting from known unspecified rotor currents set-points, oscillation-free zero dynamics trajectory are deduced, based on explicit solution of the corresponding ODE. Then the feedforward terms needed to ensure tracking of such trajectories are computed. Next the design of a saturated linear state feedback law, minimizing oscillation under dips, is defined and cast as an LMI-constrained convex optimization problem. Finally, the analytical approach for obtaining rotor current references from torque and stator reactive current is elaborated, based on the previously obtained oscillation-free zero dynamics trajectories. Numerical simulation results, obtained using Matlab/Simulink environment, are presented in Section 4 for a $0.5MW$ DFIG-based WT, to validate the proposed strategy. Some final remarks on the presented solution are discussed in Section 5.

2 Modeling and Maximum Power Point Tracking

In this Section the DFIG electromagnetic dynamic model is recalled, along with the WT mechanical dynamics. Then MPPT algorithms commonly applied in WECS are briefly sketched. These representations will be exploited in the remainder of the paper for control design and/or simulation implementation.

2.1 DFIG Model

Starting from the general DFIG three-phase model (see [18] ch. 13), under some common hypothesis [1], picking a Stator Voltage Oriented (SVO) reference frame, and rotor currents (i_{2u}, i_{2v}) and stator fluxes (ϕ_{1u}, ϕ_{1v}) as state variables, the following equivalent two-phase $(u-v)$ dynamics can be obtained as:

$$\begin{aligned}
\dot{i}_{2u} &= -\gamma_2 i_{2u} + (\omega_0 - \omega_g) i_{2v} + \beta_2 \alpha_1 \phi_{1u} - \beta_2 \omega_g \phi_{1v} - \beta_2 U + \frac{1}{\sigma_2} u_{2u} \\
\dot{i}_{2v} &= -(\omega_0 - \omega_g) i_{2u} - \gamma_2 i_{2v} + \beta_2 \omega_g \phi_{1u} + \beta_2 \alpha_1 \phi_{1v} + \frac{1}{\sigma_2} u_{2v} \\
\dot{\phi}_{1u} &= -\alpha_1 \phi_{1u} + \omega_0 \phi_{1v} + \alpha_1 L_m i_{2u} + U \\
\dot{\phi}_{1v} &= -\omega_0 \phi_{1u} - \alpha_1 \phi_{1v} + \alpha_1 L_m i_{2v} \\
T_g &= \eta_2 (\phi_{1v} i_{2u} - \phi_{1u} i_{2v})
\end{aligned} \tag{1}$$

where U is the line voltage amplitude [2], ω_g, ω_0 are the rotor and line angular speeds, respectively. T_g is the electromagnetic torque, while u_{2u}, u_{2v} are the rotor voltages. The coefficients appearing above are defined as:

$$\begin{aligned}
&\sigma_2 = L_2 \left(1 - \frac{L_m^2}{L_1 L_2}\right), \beta_2 = \frac{L_m}{\sigma_2 L_1}, \alpha_1 = -\frac{R_1}{L_1} \\
&\gamma_2 = \left(\frac{R_2}{\sigma_2} + \alpha_1 \beta_2 L_m\right), \ \eta_2 = \frac{2 n_p L_m}{3 k^2 L_1} \ .
\end{aligned} \tag{2}$$

Note that stator fluxes can be easily obtained from currents measurements as:

$$\begin{bmatrix} \phi_{1u} \\ \phi_{1v} \end{bmatrix} = L_1 \begin{bmatrix} i_{1u} \\ i_{1v} \end{bmatrix} + L_m \begin{bmatrix} i_{2u} \\ i_{2v} \end{bmatrix} . \tag{3}$$

The electrical parameters in (2) are defined in Tab. 5 in the Appendix, with numerical values referred to a $0.5MW$ DFIG.

2.2 Wind Turbine Model

For what concerns the WT mechanical behavior, the ensuing standard two-mass representation, depicted in Fig.2, is adopted

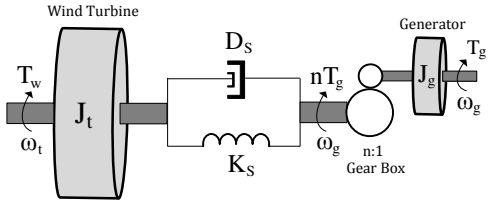

Fig. 2: Two-mass wind turbine model with gearbox.

$$\begin{aligned}
\dot{\theta}_d &= \frac{\omega_g}{n} - \omega_t \\
\dot{\omega}_t &= \frac{1}{J_t}\left(T_w(\omega_t, \beta, V_w) + K_s \theta_d + D_s\left(\frac{\omega_g}{n} - \omega_t\right)\right) \\
\dot{\omega}_g &= \frac{1}{J_g}\left(-K_s \frac{\theta_d}{n} - \frac{D_s}{n}\left(\frac{\omega_g}{n} - \omega_t\right) - T_g\right)
\end{aligned} \tag{4}$$

where indexes t, and g refer to the turbine and generator variables, respectively. Thus, ω_t and ω_g are the corresponding angular speeds, and J_g and J_t are inertias. $\theta_d = \theta_t - \frac{\theta_g}{n}$ is the drive-train low speed shaft torsional displacement, n is the gearbox ratio, while D_s and K_s are the low speed shaft damping and stiffness coefficients. The generator torque T_g is given by the last equation in (1), while the aerodynamic torque T_w can be expressed as:

$$T_w(\omega_t, \beta, V_w) = \frac{1}{2} \frac{\rho \pi R_w^3 V_w^2 C_P(\lambda, \beta)}{\lambda} \text{ with } \lambda = \frac{\omega_t R_w}{V_w} \tag{5}$$

where ρ is the air density, R_w the blades radius, while λ is the so-called tip speed ratio and β the blade pitch angle. All the WT parameters are defined in Tab. 5 in the Appendix.

[1] Linear magnetic circuits, negligible iron losses and end-windings effects.

[2] In the considered frame u-axis is aligned to the stator voltage vector which corresponds to the line voltage vector.

C_P is the power coefficient which, for standard horizontal axis WT, can be approximated as [19]:

$$C_P = 0.22\left(\frac{116}{\lambda_i} - 0.4\beta - 5\right)e^{-\frac{12.5}{\lambda_i}},\ \lambda_i = \frac{1}{\frac{1}{\lambda+0.08\beta} - \frac{0.035}{\beta^3+1}}. \tag{6}$$

Extracting the maximum wind power is the main goal for WECS. If the blade characteristic is accurately known, for a given wind speed V_w, the turbine speed allowing to extract the maximum power is $\omega_{t-opt} = \frac{\lambda_{opt}V_w}{R_w}$, where λ_{opt} is the value maximizing the coefficient C_P, in (6) for $\beta = 0$ [3]. Then, substituting in (4), the following generator torque reference can be set: $T_g^* = \frac{K_{opt}\omega_r^2}{n}$, with $K_{opt} = \frac{1}{2}\rho R_w^5 \frac{C_{Pmax}}{\lambda_{opt}}$ [20]. Otherwise, ω_{t-opt} can be adaptively retrieved by hill-climbing algorithms [21]. In the remainder of the paper, known blade aerodynamics will be assumed. Whenever generator power/torque saturation is hit (in case of strong wind), then the torque reference is frozen to the saturation value and the turbine speed is regulated by the pitch system [10]. For brevity, pitch control will not be elaborated here.

3 Control Strategy

Here the control strategy, devoted to make DFIG-based wind turbine to cope with severe voltage faults, is elaborated. As mentioned in the Introduction, the focus is put on rotor-side control, which is crucial to achieve proper generator performance. Grid side control is handled by means of standard solutions, and details will not be reported for sake of brevity, and the interested readers are referred to [7], [22].

Before detailing rotor-side controller structure, specifications to be met both in nominal and faulty conditions need to be introduced.

In this respect, DFIG's objectives are usually formulated in terms of torque, and stator-side reactive current reference values [4]. The first is given by the last equation in (1), while the second can be expressed from (3) as:

$$i_{1v} = \frac{\phi_{1v} - L_m i_{2v}}{L_1}. \tag{7}$$

References on such variables need to be mapped into corresponding trajectories for the state variables in (1), namely rotor currents and stator fluxes. In principle, there are infinite possibilities, as two trajectories must be converted into four state variables references. However, only two control inputs are available, thus the state evolution cannot be arbitrarily imposed [5]. In addition, the ensuing constraints, stemming from the machine physical limits, have to be accounted for: rotor current limits, given by RSC power switches ratings, flux linkage bounds (due to magnetic core saturation), and rotor voltages limitation, again related to RSC power electronics sizing.

Beside such nominal operation goals, a "graceful behavior" has to be guaranteed under grid faults, limiting oscillations, particularly for rotor currents, and ensuring a proper tracking of T_g and i_{1v} set points. To keep the oscillations small, state references should be suitably adapted to line voltage disturbances. This will be shown to be crucial for preventing DFIG's disconnection during voltage dips. Clearly, a proper control unit, has to be designed for tracking the aforementioned references. Here, the problem is tackled as follows: first known rotor current references, related to torque and reactive power set points, are assumed to design stator flux trajectories meeting objectives and constraints mentioned before. Based on such references suitable feedforward control actions are generated. Then, a state feedback unit is combined to these to provide robustness, and further minimize oscillations under faults, accounting for bounds on control inputs (rotor voltages).

To achieve improved tracking under voltage dips, in 3.3, a method to perform exact mapping from the original torque and reactive power references (assumed to belong to specific class of functions) to rotor current set points is elaborated. In Section 4, it will be shown how such procedure allows to achieve better torque accuracy, particularly when abrupt decrease due to line dips is required, making it a not negligible part of the overall proposed solution.

3.1 Trajectory Planning and Feedforward Action Generation

As mentioned, here known rotor currents references (i_{2u}^*, i_{2v}^*) are assumed. Then, it remains to determine suitable trajectories $(\phi_{1u}^*, \phi_{1v}^*)$ for stator fluxes, whose dynamics in (1), can be recognized as the system internal ones [23]. Assuming perfect rotor currents tracking, the corresponding zero dynamics, w.r.t. current outputs, of system (1) reads as:

$$\begin{aligned} \dot{z}_{2u} &= -\alpha_1\phi_{1u} + \omega_0\phi_{1v} + \alpha_1 L_m i_{2u}^* + U \\ \dot{z}_{2v} &= -\omega_0 z_{2u} - \alpha_1 z_{2v} + \alpha_1 L_m i_{2v}^* \end{aligned} \tag{8}$$

[3] Clearly the maximum power is obtained without pitching the blades.

[4] Tipically, Grid Codes specify LVRT reactive power support capability in terms of capacitive stator current requirements [10].

[5] Some dependencies arise, related to the system relative degree with respect to control inputs, and the form of the corresponding internal dynamics.

where, to keep consistency with the zero dynamics notation, we have defined: $z_{2u} = \phi_{1u},\ z_{2v} = \phi_{1v}$. ODEs (8) define a second order asymptotically stable LTI system which, given the typical machine parameter values (small α_1) exhibits poorly damped oscillatory modes at $-\alpha_1 \pm j\omega_0$. This feature, combined with the fact that line voltage drives dynamics (8) as an exogenous input, formally motivates the DFIG critical sensitivity to line voltage perturbations. However, among solutions of (8), it is possible to select those with no natural oscillations which, as reported in the following, are related to the forced steady-state response under inputs (i^*_{2u}, i^*_{2v}, U). Solutions of the (linear) system (8) can be analytically expressed:

$$\begin{bmatrix} z_{2u}(t) \\ z_{2v}(t) \end{bmatrix} = \begin{bmatrix} z_{1u}(0) \\ z_{1v}(0) \end{bmatrix} e^{At} + \int_0^t e^{A(t-\tau)} f(\tau) d\tau$$
$$\text{with } f(t) = \begin{bmatrix} \alpha_1 L_m i^*_{2u}(t) + U(t) \\ \alpha_1 L_m i^*_{2v}(t) \end{bmatrix}, \quad A = \begin{bmatrix} -\alpha_1 & \omega_0 \\ -\omega_0 & -\alpha_1 \end{bmatrix}. \tag{9}$$

Applying integration by parts iteratively to (9), the following equivalent expression is obtained (see [17] for details):

$$\begin{bmatrix} z_{2u}(t) \\ z_{2v}(t) \end{bmatrix} = \underbrace{\left(\begin{bmatrix} z_{2u}(0) \\ z_{2v}(0) \end{bmatrix} + \sum_{k=0}^{\infty} A^{-(k+1)} f^{(k)}(0) \right) e^{At}}_{\text{free and transient forced response}} - \underbrace{\left(\sum_{k=0}^{\infty} A^{-(k+1)} f^{(k)}(t) \right)}_{\text{forced steady-state response.}}. \tag{10}$$

This way, the free response and the transient part of the forced one, exhibiting oscillatory modes, are separated from the forced steady-state terms which are oscillation-free. Then, it is always possible to cancel out the free and forced transient responses by selecting proper initial conditions. Therefore, forced steady-state part is a trajectory for (8), with no natural oscillations. Using such solution as a reference is thus expected to prevent troubles with voltage dips. To operatively exploit (10), assumptions on the class of input functions need to be made, in order to bound the number of their not null time derivatives. In the remainder of the paper, current references and the line voltage U will be assumed bounded piece-wise linear signals, i.e. derivatives from second order on will be assumed null [6]. Summarizing all these reasoning, the stator flux references are selected as:

$$z^*_{2u}(t) = K_{1u} i^*_{2u} + K_{2u} i^*_{2v} + K_{3u} U + K_{4u} \dot{i}^*_{2u} + K_{5u} \dot{i}^*_{2v} + K_{6u} \dot{U},$$
$$z^*_{2v}(t) = K_{1v} i^*_{2u} + K_{2v} i^*_{2v} + K_{3v} U + K_{4v} \dot{i}^*_{2u} + K_{5v} \dot{i}^*_{2v} + K_{6v} \dot{U} \tag{11}$$

where all the "K-coefficients", depending on system parameters, are reported in Tab. 5 in the Appendix. To compute trajectories above, $\dot{U}$ is needed. For this purpose, and to estimate the line angle for the $u-v$ frame, a suitable observer will be adopted [7]. Finally, based on (11), and known current references, the ensuing feedforward control terms are defined

$$u_{2uff} = \sigma_2 \left(\gamma_2 i^*_{2u} - (\omega_0 - \omega_g) i^*_{2v} - \alpha_1 \beta_2 z^*_{2u} + \beta_2 \omega_g z^*_{2v} + \beta_2 U + \dot{i}^*_{2u} \right),$$
$$u_{2vff} = \sigma_2 \left(\gamma_2 i^*_{2v} + (\omega_0 - \omega_r) i^*_{2u} - \alpha_1 \beta_2 z^*_{2v} - \beta_2 \omega_g z^*_{2u} + \dot{i}^*_{2v} \right). \tag{12}$$

Beside the open loop law above, it can be proved to provide global asymptotic stability, in order to achieve robustness against parametric uncertainties, and further tame oscillations during faults, a feedback term needs to be designed. This part is specified in the next paragraph.

3.2 State Feedback Design

To improve the performance of the proposed controller under voltage sags, controller (13) is modified as:

$$u_{2u} = u_{2uff} + v_u,\ u_{2v} = u_{2vff} + v_v$$
$$\underbrace{\begin{bmatrix} v_u \\ v_v \end{bmatrix}}_{v} = \sigma(p) = \begin{bmatrix} sat(p_u) \\ sat(p_v) \end{bmatrix},\ p = K\tilde{x}_a \tag{13}$$

where a saturated linear feedback law v on the augmented (with integral terms on currents) state error $\tilde{x}_a = \left[\underbrace{\tilde{\phi}_{1u}\ \tilde{\phi}_{1v}\ \tilde{i}_{2u}\ \tilde{i}_{2v}}_{\tilde{x}} \underbrace{\int \tilde{i}_{2u} \int \tilde{i}_{2v}}_{\tilde{\chi}} \right]^T$, needs to be tuned to further limit oscillations during dips. Bounds on v can be determined as $v_{jmax} = u_{2jmax} - u_{2jffmax},\ j = u, v$ where u_{2jmax} are given by RSC ratings and $u_{2jffmax}$ by upper bounds on the feedforward effort in some worst case scenarios.

By some computations, using (12)-(13) and (1), state feedback design can be performed on the following linear, input-saturated error dynamics:

$$\dot{\tilde{x}}_a = F(t)\tilde{x}_a + G\sigma(K\tilde{x}_a),\ \text{with } \tilde{x} = C\tilde{x}_a. \tag{14}$$

where $F(t)$ is related to the right autonomous side of (1) depending on the time-varying rotor speed $\omega_g(t)$. Then, by means of modern saturated feedback design techniques and differential inclusion arguments to deal with time-varying systems, matrix K satisfying the aforementioned goals can

[6] Details about the kind of torque and reactive power signals which can be generated with this approximation are given in paragraph 3.3.

[7] Details are not reported here for brevity, the interested reader is referred to [24].

be obtained by solving the following optimization problem (see [17] for details):

$$\begin{aligned}
&\min_{Q=Q^T>0,\delta>0,Y,Z} \delta, \text{ subject to}\\
&C^TQC \le \delta I_{n\tilde{x}}\\
&QF_k^T + F_kQ + GD_iY + GD_i^-Z + Y^TD_iG^T + Z^TD_i^-G^T < 0,\\
&k = \{min, max\},\ i \in [1,4]\\
&\begin{bmatrix} Q & Z_j^T \\ Z_j & v_{jmax}^2 \end{bmatrix} \ge 0\ j = u, v,\ Q - R^{-1} \ge 0.
\end{aligned} \tag{15}$$

and recovering K as $K = YQ^{-1}$.

3.3 Reference Mapping for Improved Tracking

As mentioned, beside keeping the oscillations limited, for LVRT it is important to precisely track the varying torque and capacitive current under line faults. However, rotor currents are typically steered by means of RSC control. In this part, a precise mapping from the original torque and reactive current references into the corresponding currents references (i_{2u}^*, i_{2v}^*) is designed and analytically solved, taking into account the zero dynamics solutions obtained for the desired oscillation-free trajectories in (11). The rationale behind this approach is the following: improved tracking cannot be achieved without a suitable planning of the system zero dynamics, otherwise high flux oscillations would arise inducing core saturation and downgrading the system behavior [8]. Therefore, the zero dynamics reference planning has to be preserved. To improve tracking results w.r.t. what in [17] (and commonly applied in the literature), first-order time derivatives of all the signals involved are considered leading to a non trivial system of nonlinear equations which is analytically solved. Starting with torque, assuming a known reference T_g^* (provided from the MPPT solution recalled in 2), by the last equation of (1), we can write:

$$\begin{aligned}
T_g^* &= \eta_2(z_{2v}^* i_{2u}^* - z_{2u}^* i_{2v}^*)\\
\dot{T}_g^* &= \eta_2(\dot{z}_{2v}^* i_{2u}^* + z_{2v}^* \dot{i}_{2u}^* - \dot{z}_{2u}^* i_{2v}^* - z_{2u}^* \dot{i}_{2v}^*).
\end{aligned} \tag{16}$$

Now, the desired stator flux trajectories obtained in (11), and their first-order time derivatives can be replaced in (16) to express the torque set point and its derivative only as a function of the rotor current references, and line voltage U. Recalling the hypothesis of piecewise linear rotor currents made to derive references (11), and assuming the same for U (corresponding to a trapezoidal dip shape approximation) leads to:

$$\begin{aligned}
\dot{z}_{2u}^* &= K_{1u}\dot{i}_{2u}^* + K_{2u}\dot{i}_{2v}^* + K_{3u}\dot{U},\\
\dot{z}_{2v}^* &= K_{1v}^*\dot{i}_{2u}^* + K_{2v}\dot{i}_{2v}^* + K_{3v}\dot{U}.
\end{aligned} \tag{17}$$

Substituting the expressions above, as well as the zero dynamics trajectories from (11), into (16), the equations describing the torque reference and its derivative based on rotor currents, stator voltage, and their first-order derivatives read as:

$$\begin{aligned}
&-\frac{T}{\eta_2} + (K_{3v}U + K_{6v}\dot{U})i_{2u}^* - (K_{3u}U + K_{6u}\dot{U})i_{2v}^* + K_{1v}{i_{2u}^*}^2 +\\
&+ (K_{2v} - K_{1u})i_{2u}^* i_{2v}^* - K_{2u}{i_{2v}^*}^2 + K_{4v}i_{2u}^*\dot{i}_{2u}^* - K_{5u}i_{2v}^*\dot{i}_{2v}^* +\\
&- K_{4u}\dot{i}_{2u}^* i_{2v}^* + K_{5v}\dot{i}_{2v}^* i_{2u}^* = 0
\end{aligned} \tag{18}$$

$$\begin{aligned}
&-\frac{\dot{T}}{\eta_2} + 2K_{1v}\dot{i}_{2u}^* i_{2u}^* - 2K_{2u}\dot{i}_{2v}^* i_{2v}^* + (K_{2v} - K_{1u})\dot{i}_{2u}^* i_{2v}^* + K_{3v}\dot{U}i_{2u}^* +\\
&+ (K_{2v} - K_{1u})\dot{i}_{2v}^* i_{2u}^* + (K_{5v} - K_{4u})\dot{i}_{2u}^*\dot{i}_{2v}^* + K_{4v}(\dot{i}_{2u}^*)^2 +\\
&+ (K_{3v}U + K_{6v}\dot{U})\dot{i}_{2u}^* - K_{3u}\dot{U}i_{2v}^* - (K_{3u}U + K_{6u}\dot{U})\dot{i}_{2v}^* -\\
&+ K_{5u}(\dot{i}_{2v}^*)^2 = 0.
\end{aligned} \tag{19}$$

Similar reasoning can be made for what concerns the mapping reactive stator current reference i_{1v}^*, which, recalling (7), can be written as: $i_{1v}^* = \frac{z_{2v}^* - L_m i_{2v}^*}{L_1}$. Again, substituting z_{2v}^* according to (11), the intended equation for i_{1v}^* is attained as:

$$\begin{aligned}
&-L_1 i_{1v}^* + K_{3v}U + K_{6v}\dot{U} + K_{1v}i_{2u}^* + (K_{2v} - L_m)i_{2v}^* +\\
&+ K_{4v}\dot{i}_{2u}^* + K_{5v}\dot{i}_{2v}^* = 0.
\end{aligned} \tag{20}$$

Deriving (20), the equation expressing $\dot{i}_{1v}^*$ in terms of the unknowns $i_{i2u}^*, i_{2v}^*, \dot{i}_{2u}^*, \dot{i}_{2v}^*$ is easily obtained:

$$-L_1\dot{i}_{1v}^* + K_{3v}\dot{U} + K_{1v}\dot{i}_{2u}^* + (K_{2v} - L_m)\dot{i}_{2v}^* = 0. \tag{21}$$

From the algebraic viewpoint, we have obtained a system of four equations, including two second-order nonlinear (18), (19), and two linear ones (20), (21), relating the known variables (original references) $[T_g^*, \dot{T}_g^*, i_{1v}^*, \dot{i}_{1v}^*]$, with the set of four unknown variables $[i_{2u}^*, i_{2v}^*, \dot{i}_{2u}^*, \dot{i}_{2v}^*]$ also via the known parameters $[U, \dot{U}]$. In terms of the class of torque and reactive current signals which can be obtained by the equations above, it can be shown [9] that, assuming piecewise linear rotor currents, piecewise quadratic functions can be obtained for what concerns torque, due to the nonlinear nature of eqs. (18), (19). While piecewise linear function can be clearly achieved for what concerns i_{1v}^*. This degree of freedom is sufficient to generate the typical references arising in DFIG-based WT control application.

[8] See [17] where an example with standard feedback linearisation control is reported to underscore this fact.

[9] Owing to space constraints the mathematical details are omitted.

For what concerns the system of equations solution, the following simple procedure can be carried out: first, $\dot{i}^*_{2u}, \dot{i}^*_{2v}$ in the non-linear equations (18), (19) are replaced by the solutions (parametrized in i^*_{2u}, i^*_{2v}), of the linear equations (20), (21). This way, the torque equation and it's first-order derivative are expressed as quadratic functions of the rotor currents references. This equations can be manipulated with standard procedure [10] to obtain a fourth-order equation in one variable (e.g. i^*_{2v}), defining a *Quartic Function*, whose roots can be expressed in closed-form in terms of its coefficients. Obviously, the other variables can be retrieved substituting back such roots in the equations. From an engineering view point, we are clearly interested in real valued solutions (the nature of solutions depends on the value that the coefficients assume at a given instant). In case, there are more than one, the one providing the minimum *Euclidean norm* for the rotor current reference vector is selected. This choice stems from quite obvious energy efficiency considerations: the less the currents the lower the power dissipation by *Joule* effect is, and also the RSC electronics would be less stressed.

It is further to remark that the proposed mapping solution, beside being exact (for the class of references mentioned before), can be efficiently implemented online, for each set of the original references T^*_g and i^*_{1v}, and parameters U, $\dot{U}$. Indeed, being a closed-form solution, no iterative procedure is needed and the computational burden is reduced to the evaluation of a function providing the roots in terms of the current coefficients, and the best solution selection, according to the criterion explained above.

4 Simulation Results

To validate the proposed strategy, a $0.5MW$ DFIG-based WT system has been considered. Mechanical model parameters are reported in Tab. 5, while the DFIG coefficients are reported in Tab. 5. A PWM-driven back-to-back switching converter, providing GSC and RSC functionalities has been emulated as well, with parameters of Tab. 5. For RSC, a discrete time version of controller (13), with saturated feedback terms v_u, v_v designed according to the LMI-based procedure outlined in 3.2, has been implemented, with sampling time equal to the PWM period. The following parameters have been considered to numerically solve problem (15): $v_{jmax} = u_{2jmax}/2$, $j = u, v$, $\omega_g(t) \in [0.7\omega_{nom}, 1.3\omega_{nom}]$, with $\omega_{nom} = 2\pi 50 rad/s$ representing the synchronous speed of the machine. Initial conditions for $\tilde{x}_a$ have been assumed to belong to a unit ellipsoid defined by $R = diag(\tilde{z}^{-2}_{2u}, \tilde{z}^{-2}_{2v}, \tilde{i}^{-2}_{2u}, \tilde{i}^{-2}_{2u}, \tilde{\chi}^{-2}_{2u}, \tilde{\chi}^{-2}_{2v})$, where $\tilde{z}_{2u} = 0.25Wb, \tilde{z}_{2v} = 0.85Wb, \tilde{i}_{2u} = 100A, \tilde{i}_{2v} = 100A, \tilde{\chi}_{2u} = 10As$, $\tilde{\chi}_{2v} = 10As$ have been conservatively set according to tracking steps during the voltage sag. The resulting feedback matrix, obtained by solving (15) with these data is $K = \begin{bmatrix} 116.5 & -112.8 & 0.491 & -0.001 & 1.67 & 0.0005 \\ 191.4 & 49.14 & -0.008 & 0.679 & -0.00016 & 1.57 \end{bmatrix}$. While for the GSC, standard decoupled $d-q$ control loops have been applied [22]. Similarly, a discrete version of the observer in [24] has been implemented to get information about $U, \dot{U}$. A symmetric three-phase short-circuit fault at the PCC (as shown in Fig.1) causing a 100% stator voltage drop lasting for $150ms$, has been emulated, while system operates in the steady-state condition corresponding to nominal $10m/s$ and high $13m/s$ wind speed (the latter requiring pitching). In nominal condition, the reference torque corresponding to the maximum power point defined in Section 2, or the generator rated value in case of high wind speed, is considered, while null capacitive current is set. When the voltage sag is detected (via the line observer), the references are changed as follows: T^*_g is reduced according to the dip depth, while i^*_{1v} is increased to comply with the grid codes requirements asking to keep it above 90% of the rated value to sustain the grid voltage [4], [25]. Before showing the behavior of the system scenarios, we compare, under the aforementioned dip, the proposed mapping solution, with a steady-state mapping approach, which assumes constant rotor currents [11]. Results are portrayed in Fig. 3 for the steady-state simplified mapping, and 4 for the proposed mapping. The torque and reactive current signals constructed by means of the mapping solutions are denoted with the accent $\hat{}$.

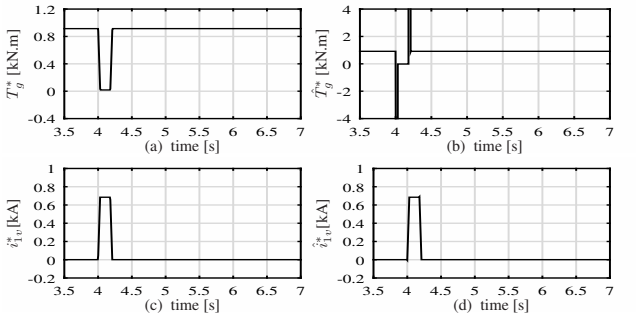

[10] E.g. combining the equations to eliminate the square terms in one of the two variables, solving for it, and replacing the roots in one of the two original equation.

[11] In this case, coefficients K_{4u}, K_{5u}, K_{4v}, K_{5v} in (11) are set to zero, and rotor currents are computed solving a standard second-order quadratic equation.

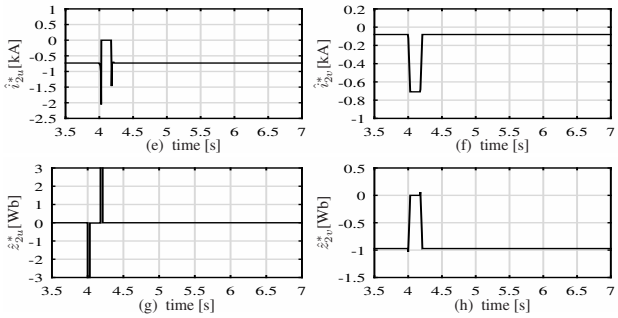

Fig. 3: Translated references by simplified mapping solution for the system under 100% voltage dip lasting for $150ms$.

By Fig.3, it is clear how ignoring the first-order derivatives of the rotor currents in the zero dynamics calculations, results in a large u-axis stator flux trajectory ($\hat{z}^*_{2u}$), beyond the machine physical limits (see Fig. 3 (g)). As a consequence, large and inconsistent translated reference torque $\hat{T}^*_g$ is obtained (see Fig. 3 (b)). Hence, the steady-state mapping is not suited for dealing with harsh line faults.

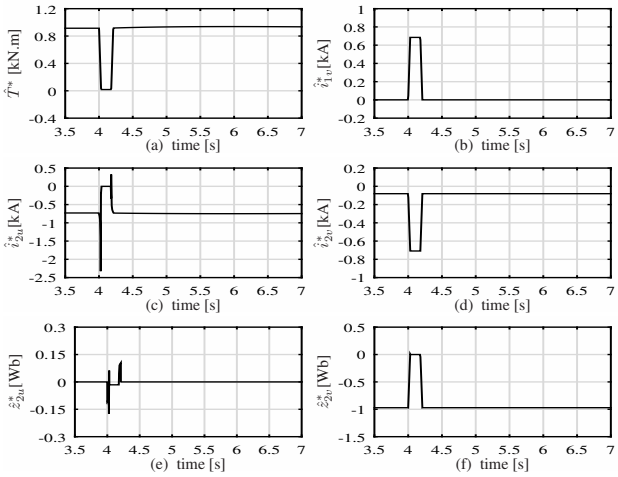

Fig. 4: Translated references by proposed mapping solution for the system under 100% voltage dip lasting for $150ms$.

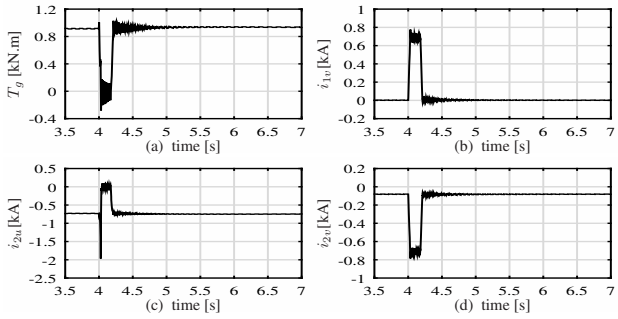

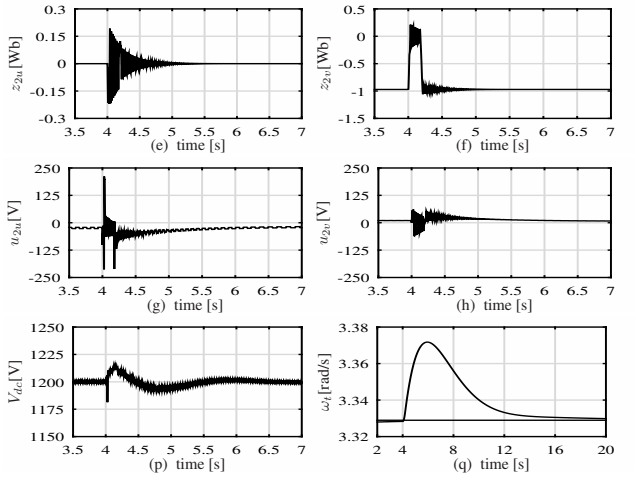

Fig. 5: Results of the system with the proposed mapping solution and control strategy, at normal wind speed ($10m/s$) under 100% symmetrical voltage dip lasting for $150ms$.

Instead, as confirmed by plots in Fig.4, references computed with the mapping solution presented in 3.3, accurately track the desired torque and capacitive stator current. As can be seen in Fig.4 (e), in contrast to the steady-state mapping, $\hat{z}^*_{2u}$ is reasonably inside the machine's physical constraints and the corresponding torque reference $\hat{T}^*_g$ computed through the mapped signals (see Fig.4 (a)), matches perfectly the desired torque reference T^*_g (see Fig.3 (a)). Therefore, the importance of the proposed improved mapping solution is underscored. Thus, in the following simulations, the proposed mapping is used to evaluate the overall system response to the voltage dip. Fig.5 illustrates results for the system operating with $10m/s$ wind speed, while facing the above-introduced grid fault. The oscillations of all the state variables are generally well below the system limits (provided in Tab. 5), as highlighted in Figs. 5 (a)-(f)). Fleeting spikes arise in the rotor current u-component (due to the slight delay in dip detection via the observer), still they are inside the peak bound for RSC electronics [12] . Moreover, they quickly vanish to the desired references, as well as the other state variables. Note that the feedback action causes saturation of the control inputs multiple times during the dip (Fig. 5 (g)), however, since saturation is explicitly considered in designing the state feedback part, a graceful behavior of the system is maintained [13] . Accurate tracking of the electromagnetic torque and reactive current references is achieved thanks to the proposed mapping. The improved mapping also has

[12] Usually two times the rotor current nominal value.

[13] It is worth noting that, due to some conservatism in the feedback part saturation bounds (half of the control effort is constantly preserved for the feedforward terms), the available rotor voltage range is not fully exploited.

positive effects in smoothing the system transient and the residual oscillations at the dip start, which are related to the fact that the actual dip shape does not perfectly fit the trapezoidal approximation adopted for calculating references in (11) and feedforward terms (12).

Fig. 5-(p) shows how also the mechanical part of the WT exhibit a smooth, non oscillatory behavior thanks to the adopted RSC control. Indeed, the turbine speed smoothly increases within the fault, (due to the torque reduction), then it converges back to the optimal pre-fault speed, avoiding excitation of the shaft resonance modes. Indeed, the frequency of residual generator torque oscillations is much higher than the drive-train resonant frequency. For what regards the grid side, as a result of the fast and proper response of the RSC to the dip, the standard GSC control keeps the transient oscillations of the DC-link voltage (V_{dc}) sufficiently damped, and the peak value at $1220V$ (see Fig. 5 (p)), inside the $+15\%$ safety margins, w.r.t. nominal operation value, typically kept when sizing the DC-bus capacitor [10, 11]. This confirms that the proposed approach can be profitably exploited for realistic applications.

Fig.6 depicts the results obtained under the previous test conditions, but for high wind speed ($13m/s$). Also in this case, the system response to the grid fault, ensures the LVRT capability. Similar to the previous test, the currents/fluxes oscillations are efficiently suppressed and proper torque, capacitive current tracking is achieved. At this wind speed, generator power saturation is hit, thus pitch control (a standard PI has been used) is activated (see Fig. 6 (s)) keeping the speed at 110% of the synchronous value [14] . During the dip, turbine speed increases as a consequence of torque reduction and the pitch actuation rate limitation, however, the generator speed is kept below the 130% synchronous speed (Fig. 6 (p)). Also in this scenario, after the dip clearance, the DFIG and WT speeds, turn back smoothly to the rated values (see Fig. 6 (p)-(q)).

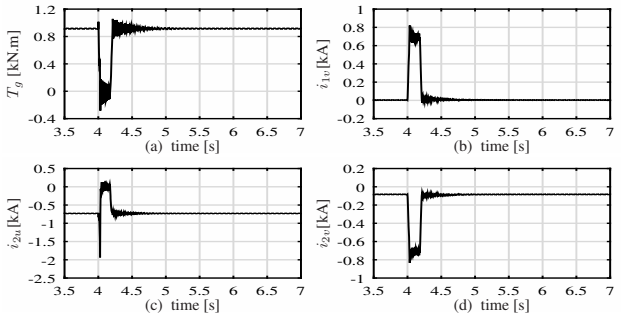

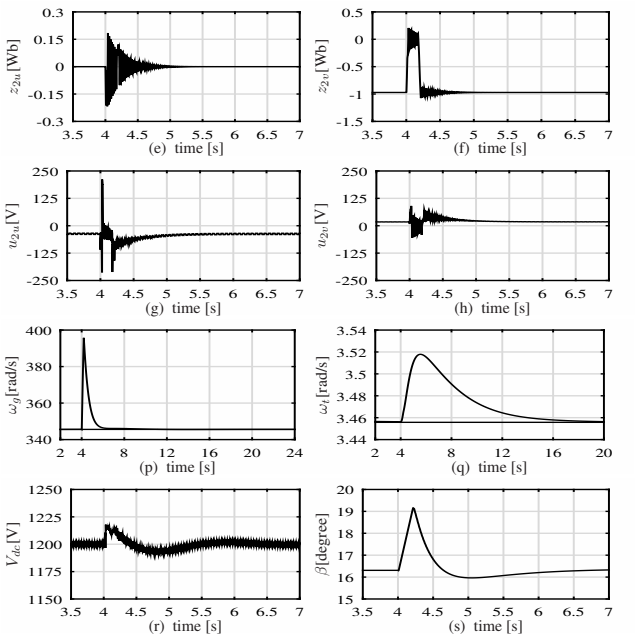

Fig. 6: Results of the system with the proposed mapping solution and control strategy, at high wind speed ($13m/s$) under 100% symmetrical voltage dip lasting for $150ms$.

5 Conclusions

In this paper, LVRT with improved tracking under grid faults has been achieved for a full benchmark of a WECS including wind turbine, DFIG, and both rotor and grid side power electronic converters. The crucial methodological elements to obtain these performance are an advanced RSC control strategy, minimizing oscillations throughout the voltage dip, and a not trivial mapping relation between the DFIG-based WT standard output variables (generator torque and capacitive stator currents during faults) and the rotor currents which are directly steered by the RSC. Validation via realistic numerical tests show promising results, confirming that the strategy can handle harsh grid faults without the intervention of additional protection hardware, thus reducing system cost and fully guaranteeing LVRT features as specified in recent Grid Codes. Despite the methodological sophistication, the overall control algorithm and mapping strategy are easy-to-implement on embedded computational platforms, as no heavy computation (e.g. optimization, iterative algorithms) is required on-line.

[14] For energy efficiency, to keep power bounded to generator nominal value, a little overspeed is allowed during pitching, so that the generator torque can be reduced [7].

References

[1] International Renewable Energy Agency (IRENA). Renewable Capacity Statistics 2016. *IRENA*, 2016.

[2] V. Yaramasu, B. Wu, P. C. Sen, S. Kouro. High power wind energy conversion systems: State-of-the-art and emerging technologies. *Proceedings of IEEE*, 2015, 103(5).

[3] A. Sureda, A. Munoz, R. Pena, R. Cardenas. Control of a Brushless Doubly-Fed induction generator via a matrix converter. *IEEE Power Electronics and Applications (EPE 2011)*, 2011.

[4] USA FERC. Interconnection for wind energy. *Docket No. RM05-4-001, Order No. 661-A*, 2005.

[5] E.ON Netz Gmbh. Grid code, high and extra high voltages *Docket No. RM05-4-001, Order No. 661-A*, 2006.

[6] F.K.A. Lima, A. Luna, P. Rodriguez, E.H. Watanabe, F. Blaabjerg. Rotor voltage dynamics in the doubly fed induction generator during grid faults. *IEEE Trans. Power Electronics*, 2010, 25(1): 118 – 130.

[7] L. Yang, Z. Xu, J. Østergaard, Z. Y. Dong, K. P.Wong. Advanced control strategy of DFIG wind turbines for power system fault ride through. *IEEE Trans. Power Syst.*, 2012, 27(2): 713 – 722.

[8] K.E. Okedu, S.M. Muyeen, R. Takahashi, J. Tamura. Wind farms fault ride through using DFIG with new protection scheme. *IEEE Trans. Sustainable Energy*, 2012, 3(3): 242 – 254.

[9] P. Baiju, T. Rajeev. Low Voltage Ride Through in DFIG based wind turbines: A review. *IEEE Inter. Conf. Ctrl. Communication and Computing India (ICCC)*, 2015.

[10] D. Xie, Z. Xu, L. Yang, J. Østergaard, Y. Xue, K. P.Wong. A Comprehensive LVRT Control Strategy for DFIG Wind Turbines With Enhanced Reactive Power Support. *IEEE Trans. Power Syst.*, 2013, 28(3): 3302 – 3310.

[11] Z. Zou, X. Xiao, Y. Liu, Y. Zhang, Y. Wang. Integrated Protection of DFIG-Based Wind Turbine With a Resistive-Type SFCL Under Symmetrical and Asymmetrical Faults. *IEEE Trans. Appl. Super.*, 2016, 26(7).

[12] Y. Shen, D. Ke, W. Qiao, Y. Sun, D. S. Kirschen, C. Wei. Transient Reconfiguration and Coordinated Control for Power Converters to Enhance the LVRT of a DFIG Wind Turbine With an Energy Storage Device. *IEEE Trans. Energy Convers.*, 2015, 30(4): 1679 – 1690.

[13] Q. Huang, X. Zou, D. Zhu, Y. Kang. Scaled Current Tracking Control for Doubly Fed Induction Generator to Ride-Through Serious Grid Faults. *IEEE Trans. Power Elect.*, 2016, 31(3): 2150 – 2166.

[14] E. Bogalecka, Z. Kzreminski. Control system of a doubly fed induction machine supplied by current controlled voltage source inverter. *Proc. of the IEEE Conf. on Electr. Machines and Drives*, 1996: 168 – 172.

[15] S. Peresada, A. Tilli, A. Tonielli. Indirect Stator Flux-Oriented Output Feedback Control of a Doubly Fed Induction Machine. *IEEE Trans. Control System Tech.*, 2003, 11(6): 875 – 888.

[16] G. Brando and L. Cozza and C. del Pizzo. Optimized Control of Active Front-Ends to Improve Efficiency and Power Quality in Systems with Closed-Loop Controlled Electrical Drives. *Springer-Verlag*, 2003, 11(6): 508 – 514.

[17] A. Tilli, C. Conficoni, A. Hashemi. State reference design and saturated control of doubly-fed induction generators under voltage dips. *International Journal of Control*, 2017, 90(4): 834 – 854.

[18] W. Leonhard. Control of electrical drives. (3rd ed.). *Springer, Berlin*, 2001.

[19] H.A. Mohammadpour and E. Santi. Modeling and Control of Gate-Controlled Series Capacitor Interfaced With a DFIG-Based Wind Farm. *IEEE Trans. Ind. Electron.*, 2015, 62(2): 1022 – 1033.

[20] F.D. Bianchi, H.D. Battista, R.J. Mantz. Wind turbine control systems: principles, modelling and gain scheduling design. *Springer Science & Business Media*, 2006.

[21] B. Shen, B. Mwinyiwiwa, Y. Zhang, B. T. Ooi. Sensorless maximum power point tracking of wind by DFIG using rotor position phase lock loop (PLL). *IEEE Trans. Power Elect.*, 2009, 24(4): 942 – 951.

[22] R. Pena, J. C. Clare, G. M. Asher. Doubly fed induction generator using back-to-back PWM converters and its applications to variable speed wind-energy generation. *Inst. Elec. Eng. Proc. Electric Power Applications*, 1996, 143(3): 231 – 241.

[23] A. Isidori. Nonlinear control systems. *Springer, Hiedelberg*, 1999.

[24] A. Tilli, C. Conficoni. Adaptive observer for three phase line voltage under unbalanced conditions. *Proc. of NOLCOS*, 2010: 1981 – 1986.

[25] J. Ruan, Z. Lu, Y. Qiao, Y. Min. Analysis on Applicability Problems of the Aggregation-Based Representation of Wind Farms Considering DFIGs LVRT Behaviors. *IEEE Trans. Power Systems*, 2016, 31(6): 4953 – 4965.

Appendix The tables below give the parameters of the studied system:

Table 1 DFIG parameters reported to the stator side.

DFIG rated power $[MW]$	0.5
DFIG rated torque T_g $[Nm]$	1000
DFIG rated RMS voltage [V]	380
DFIG rated RMS current [A]	760
RSC rated RMS voltage [V]	265
RSC rated RMS current [A]	780
Stator resistance R_1 [Ω]	0.0073
Stator inductance L_1 [H]	0.0126
Rotor resistance R_2 [Ω]	0.0073
Rotor inductance L_2 [H]	0.01255
Mutual inductance L_m [H]	0.01218
Number of pole pairs n_p	2
DFIG inertia $J_g = 2H_g$ $[kgm^2]$	4.5

Table 2 Wind turbine parameters.

Turbine rated power $[MW]$	0.5
Turbine inertia $J_t = 2H_t$ $[kgm^2]$	2.70×10^5
Shaft stiffness coefficient K_s $[Nm/rad]$	13700
Shaft damping coefficient D_s $[Nm/rad/s]$	275
Gearbox coefficient n	100
Blades radius R_w $[m]$	19
Air density ρ $[kg/m^3]$	1.225

Table 3 Zero dynamics trajectories' coefficients.

$K_{1u} = \frac{\alpha_1^2 L_m}{M}$	$K_{2u} = \frac{\alpha_1 \omega_0 L_m}{M}$	$K_{3u} = -\frac{\omega_0}{M}$
$K_{4u} = -\frac{N \alpha_1 L_m}{M^2}$	$K_{5u} = -\frac{2\alpha_1^2 \omega_0 L_m}{M^2}$	$K_{6u} = -\frac{N}{M^2}$
$K_{1v} = -\frac{\alpha_1 \omega_0 L_m}{M}$	$K_{2v} = \frac{\alpha_1^2 L_m}{M}$	$K_{3v} = -\frac{\omega_0}{M}$
$K_{4v} = \frac{2\alpha_1^2 \omega_0 L_m}{M^2}$	$K_{5v} = -\frac{N \alpha_1 L_m}{M^2}$	$K_{6v} = \frac{2\alpha_1 \omega_0}{M^2}$
$M = \alpha_1^2 + \omega_0^2$	$N = \alpha_1^2 - \omega_0^2$	

Table 4 Converters' parameters.

DC-link capacitor C $[F]$	0.06
DC-link rated voltage V_{dc} $[V]$	1200
Resistance of the grid side inductor R_g $[\Omega]$	0.866×10^{-3}
Inductance of the grid side inductor L_g $[H]$	0.0866
PWM switching frequency $[Hz]$	2.5×10^3

Ahmad HASHEMI was was born in Kermanshah, Iran, in July 1984. He received the Bachelor's and Master's degrees in Electrical Engineering from K.N.Toosi University of Technology, Tehran, Iran, and Madani University, Tabriz, Iran, in 2006 and 2009, respectively. In 2014, he started his Ph.D. in Automatic Control with the Department of Electrical, Electronic and Information Engineering (DEI), University of Bologna, Italy. He was a visiting Ph.D. student with the Department of Electromagnetic Engineering, KTH Royal Institute of Technology, Sweden, in 2017. His current research interests include modeling, control and applications of the FACTS devices and renewable energy generation systems. E-mail: ahmad.hashemi@unibo.it.

Andrea Tilli is Associate Professor at the Department of Electrical, Electronic and Information Engineering "Guglielmo Marconi" (DEI) of the University of Bologna. In 2000, he received the Ph.D. degree in system science and engineering from the same university. He is member of the Center for Research on Complex Automated Systems "Giuseppe Evangelisti" (CASY), established within DEI. His current research interests include applied nonlinear control techniques, active power filters, wind turbines, electric drives for motion control and energy generation, thermal control of many-core systems-on-chip and supercomputers. E-mail: a.tilli@unibo.it.

Christian Conficoni Received the Master's Degree in Electronic Engineering, from the University of Bologna, Italy in 2008. In 2013 he received the Ph.D. degree in automatic control, from the same institution. Currently he is a post doctoral researcher at the Department of Electrical, Electronic and Information Engineering (DEI), at University of Bologna. His research interests include applied nonlinear control solutions for power electronic and electromechanical systems oriented to power quality enhancement, adaptive observers for electric drives sensorless operation, modeling and energy-oriented optimal thermal management of advanced computing platforms. E-mail: christian.conficoni3@unibo.it.